

Journal of Materials Chemistry A

Accepted Manuscript



This is an *Accepted Manuscript*, which has been through the Royal Society of Chemistry peer review process and has been accepted for publication.

Accepted Manuscripts are published online shortly after acceptance, before technical editing, formatting and proof reading. Using this free service, authors can make their results available to the community, in citable form, before we publish the edited article. We will replace this *Accepted Manuscript* with the edited and formatted *Advance Article* as soon as it is available.

You can find more information about *Accepted Manuscripts* in the [Information for Authors](#).

Please note that technical editing may introduce minor changes to the text and/or graphics, which may alter content. The journal's standard [Terms & Conditions](#) and the [Ethical guidelines](#) still apply. In no event shall the Royal Society of Chemistry be held responsible for any errors or omissions in this *Accepted Manuscript* or any consequences arising from the use of any information it contains.

Cite this: DOI: 10.1039/c0xx00000x

www.rsc.org/xxxxxx

ARTICLE TYPE

Efficient Hole-Conductor-Free, Fully Printable Mesoscopic Perovskite Solar Cells with a Broad Light Harvester $\text{NH}_2\text{CH}=\text{NH}_2\text{PbI}_3$

Min Hu, Linfeng Liu, Anyi Mei, Ying Yang, Tongfa Liu, Hongwei Han*

Received (in XXX, XXX) XthXXXXXXXXXX 20XX, Accepted Xth XXXXXXXXXXXX 20XX

DOI: 10.1039/b000000x

Formamidinium lead trihalide perovskite (FAPbI₃) was successfully introduced into the hole-conductor-free fully printable mesoscopic perovskite solar cells with carbon counter electrode. With sequential deposition method, FAPbI₃ based solar cell yielded an efficiency of 11.9%, superior to methylammonium lead trihalide perovskite (MAPbI₃) solar cell of 11.4%, which is due to broadening of the light to 840 nm. By optimizing the formamidinium and methylammonium cations mixing ratio to 3:2, power conversion efficiency of 12.9% was achieved with this low-cost fully printable mesoscopic solar cell, which indicated a promising prospect for low-cost photovoltaic technology.

Introduction

Over the last two years, hybrid organic-inorganic perovskite solar cells have distinguished themselves as an impressively efficient, inexpensive photovoltaic technology.¹⁻⁶ By cooperating with Spiro-OMeTAD as the hole-transporting material (HTM) and methylammonium lead trihalide perovskite (MAPbI₃) as the light-harvester, a certified power conversion efficiency (PCE) of 17.9% has been shot up in the early 2014, making it a potential candidate for solid-state photovoltaic devices.⁷

To fulfil the requirement of the commercial application, two of the most important issues in perovskite solar cells should be addressed.⁸⁻¹⁰ First of all, the use of HTMs bears a large proportion of cost and device stability for such solar cells, limiting their approach to low-cost photovoltaic devices. Fortunately, the ambipolar property of perovskite makes it act as both electron and hole-transporting material in the solar cells. Thus, HTM-free structured mesoscopic solar cells emerged and developed recently, and PCEs over 10% were reported both by our and other groups.¹¹⁻¹⁵ Secondly, most of the perovskite solar cells employed noble metal Au or Ag as counter electrodes (CEs), prepared by thermal evaporation under high vacuum condition, which is highly energy-consuming and complicated. Therefore, it is necessary to replace the evaporated metal (Au/Ag) electrode with low cost materials to reduce the cost of solar cell fabrication and realize large-scale fabrication. As alternative electrodes, carbon based electrodes have been widely investigated due to their low cost, easy preparation and screen printable deposition for large scale production.¹⁶⁻¹⁸ Previously, we have developed mesoscopic MAPbI₃ perovskite solar cells with low-cost carbon CE and fully printable process.¹⁴⁻¹⁵ By tuning the morphology of mesoporous carbon CEs and the TiO₂ scaffold, highly efficient mesoscopic perovskite solar cells were obtained. The PCE of 10.64% encouraged us to further optimize this type of perovskite solar cell.

To date, the most-studied perovskite light-harvesters are MAPbI₃ and MAPbI_{3-x}Cl_x, which have a bandgap of approximately 1.55 eV, giving light absorption across most of the solar spectrum to 800 nm.⁶ Nevertheless, it is known that the optimal bandgap for a single junction solar cell is between 1.1 and 1.4 eV,¹⁹ currently beyond the range of the MAPbI₃ system. One effective method is to mix PbI₂ with SnI₂ to form CH₃NH₃Sn_xPb_(1-x)I₃, which obtained the band gap as low as 1.1 eV. The edge of the incident-photon-to-current efficiency (IPCE) curve extended to 1060nm.²⁰⁻²² However, Sn²⁺ would be oxidized to Sn⁴⁺ in the atmosphere easily, which damages the optical and photovoltaic properties of this material, and hinders its practical application. Another strategy is to substitute the organic cations, and it was demonstrated that the enlargement of the octahedral network influenced the bandgap of the perovskite effectively. Recently reported formamidinium cation (HC(NH₂)₂⁺, FA) is slightly larger than methylammonium (CH₃NH₃⁺, MA), and proved to form the 3D perovskite sufficiently with a lower bandgap of about 1.47 eV. An average PCE of 9.7% and the highest PCE of 14.2% were reported based on a planar FAPbI₃ perovskite structure without having a porous TiO₂ layer. By combining MAI with FAI in sequential deposition method, the efficiencies of 14.9% and 16.01% were obtained.²³⁻²⁷

To increase the short-circuit current density (J_{SC}) and thus enhance the efficiency of hole-conductor-free mesoscopic perovskite solar cells with carbon CE, we attempted to introduce formamidinium lead trihalide perovskite (FAPbI₃) into the solar cell to broaden the light-harvesting area. It was demonstrated that the IPCE of the solar cell with pure FAPbI₃ light harvester was extended to 840 nm and the J_{SC} was improved from 17.5 mA cm⁻² to 18.4 mA cm⁻² compared with that of MAPbI₃ based solar cell by sequential deposition method. PCE of 11.9% was achieved for FAPbI₃ perovskite solar cell, which is superior to MAPbI₃ with PCE of 11.4%. By optimizing the FAI and MAI cations mixing

ratio being 3:2, an optimal PCE of 12.9% was reached due to the enhanced short-circuit current density and a little loss of FF and open-circuit voltage (V_{OC}). These results indicated a promising prospect for low-cost photovoltaic technology.

5 Experimental section

Synthesis of MAI and FAI. MAI and FAI were prepared according to literatures.^{25, 28} MAI was synthesized by adding 27 mL methylamine into 30 mL HI (57 wt% in water) at 0 °C for 2 hours with stirring. After removing the solvent, the product was washed with diethyl ether and then recrystallized with ethanol. The white crystals were obtained and dried in a vacuum box. FAI was synthesized by adding 3 g formamidine acetate into 13 mL HI (57 wt% in water), and stirring for half an hour at 50 °C. The solvent was removed by rotary evaporator, and the yellow precipitate was washed several times with diethyl ether, which was followed by recrystallization with ethanol. The white crystals were obtained and dried in a vacuum box.

Fabrication of mesoscopic perovskite solar cells based on carbon CE. FTO glass was etched with a laser to form two detached electrode pattern before being ultrasonically cleaned with detergent, deionized water and ethanol successively. Subsequently, the patterned substrates were coated with a roughly 100 nm compact TiO_2 layer by aerosol spray pyrolysis at 450 °C. After cooling down to room temperature naturally, a TiO_2 nanocrystalline layer (PASOL HPW-18NR) was deposited on top of the compact layer by screen printing and then sintered at 500 °C for 30 min. After that, a ZrO_2 spacer layer and a 10 μm mesoscopic carbon layer were printed on the top of the TiO_2 nanocrystalline layer successively, and then the films were sintered at 400 °C for 30 min. The ZrO_2 and carbon slurries were prepared as we reported previously.¹⁴⁻¹⁵ The deposition of perovskite into TiO_2/ZrO_2 /carbon three mesoscopic porous films was achieved by a two-step sequential deposition method, and the illustration of device fabrication process with sequential deposition method is shown in Figure 1c. Firstly, the porous films were infiltrated with PbI_2 by drop-coating 1.5 μL PbI_2 solution (1.1M, namely 0.507g PbI_2 was dissolved in 1mL DMF by heating at 70 °C overnight) on the top of the carbon layer. After drying at 70 °C for 30 minutes, the films coated with PbI_2 were dipped in a solution of MAI or FAI (both the concentrations are 0.063 M) in isopropanol for 15 minutes. The colour of the films would change from yellow to dark brown when perovskite formed. After that, the films were rinsed with isopropanol to remove unreacted MAI or FAI, followed by a heating treatment at 70 °C for another 30 minutes. All the reagents were purchased from Aldrich and used without further purification. All the procedures above were completed in air conditions.

Characterization. The thickness of the films was measured with a profilometer (VeecoDektak 150). The X-ray diffraction (XRD) spectra were obtained using a Bruker D8 Advance X-ray diffractometer with Cu K α radiation ($\lambda = 1.5418 \text{ \AA}$). Absorption measurement was performed by a UV-vis Spectrophotometer (Lambda 950, PerkinElmer). The cross section of the devices and the carbon films were imaged by a field-emission scanning electron microscope (FE-SEM). Photocurrent density-voltage ($J-V$) characteristics were measured using a Keithley 2400 sourcemeter and a Newport solar simulator (model 91192-1000)

giving light with AM 1.5G spectral distribution. A black mask with a circular aperture (0.07 cm^2) smaller than the active area of the square solar cell (0.5 cm^2) was applied on top of the cell. The scan rate was 250 $mV s^{-1}$ and the scan direction was from open-circuit to short circuit. The incident photon conversion efficiency (IPCE) was measured using a 150 W xenon lamp (Oriel) fitted with a monochromator (Cornerstone 74004) as a monochromatic light source. The impedance measurements were performed using a potentiostat (EG&G, M2273) in the dark. The frequency range was from 1 MHz to 100 mHz.

Results and Discussion

The schematic of a typical hole-conductor-free mesoscopic solar cell based on a carbon CE is presented in Figure 1a.^{14, 29} All of the films in the mesoscopic solar cell were fabricated by screen-printing technology including the mesoscopic carbon CE. A point worth emphasizing is that the TiO_2 film and the mesoscopic carbon CE were separated by the mesoporous ZrO_2 layer, ensuring that there was no threat of direct contact between the photoanode and CE. Moreover, the series resistance of the device was controlled by the thickness of the porous ZrO_2 layer with the technology of screen-printing.¹⁵

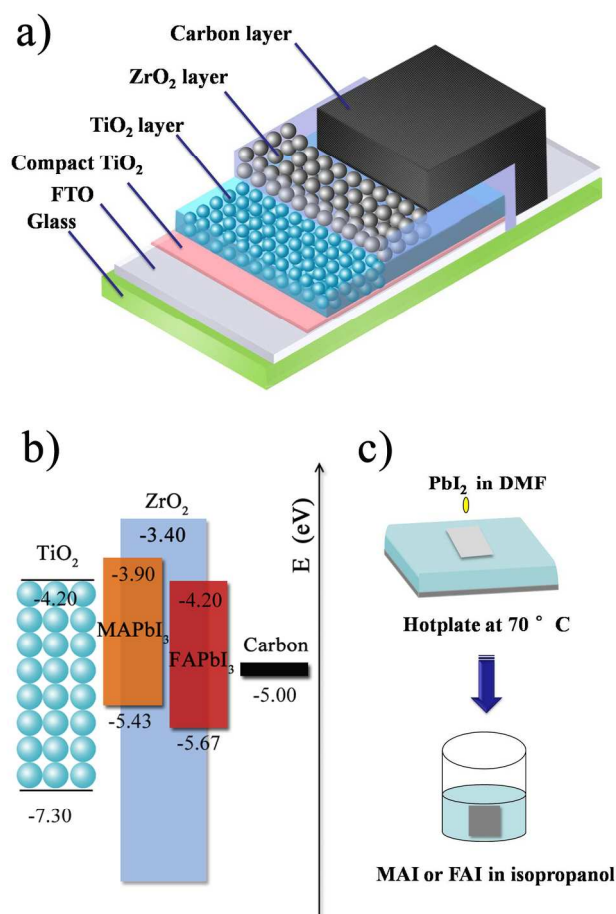


Figure 1 (a) The schematic structure of fully printable mesoscopic perovskite solar cell with carbon counter electrode; (b) The energy level diagram of the pure $MAPbI_3$ and $FAPbI_3$ perovskites; (c) The schematic illustration of sequential deposition method.

The energy level diagram is presented in Figure 1b, and the positions of the energy levels are according to the literature.⁶ The valence band of the perovskite, MAPbI₃ and FAPbI₃ are -5.43 eV and -5.67 eV vs. vacuum energy respectively, which are lower than the work function of our carbon counter electrode (about -5.0 eV).¹⁴ Thus, it is energetically favourable for the holes transporting through the perovskite layer and collecting by the carbon CE. The conduction band of TiO₂ is about -4.20 eV, allowing both pure MAPbI₃ and FAPbI₃ to inject electrons into TiO₂. The conduction band of ZrO₂ is -3.4eV, higher than that of TiO₂, MAPbI₃ and FAPbI₃ perovskite, which makes ZrO₂ block photoexcited electrons to reach the back contact.

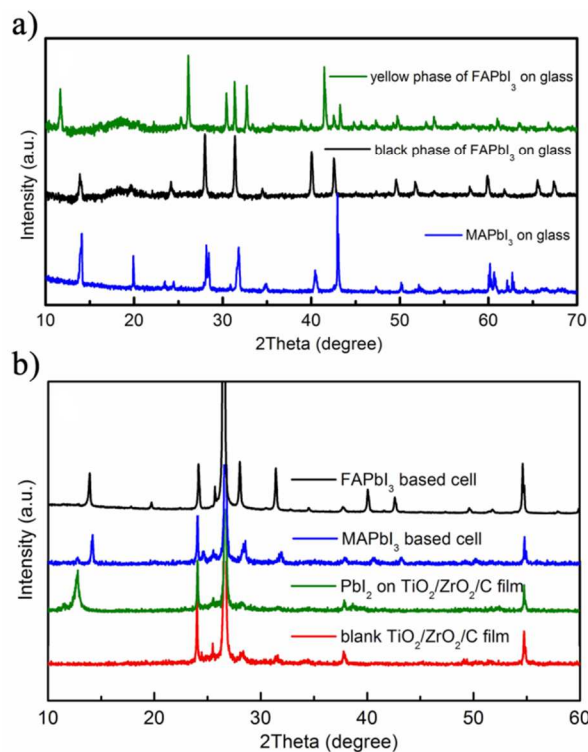


Figure 2 (a) The XRD spectra of MAPbI₃ and FAPbI₃ on the glass substrate; (b) The XRD spectra of blank TiO₂/ZrO₂/carbon film and PbI₂ in TiO₂/ZrO₂/carbon film, MAPbI₃ and FAPbI₃ based cells by sequential deposition method.

The XRD spectra of MAPbI₃ and FAPbI₃ with one-step method on the glass substrate are shown in Figure 2a. The sharp diffraction peaks indicate the high crystallinity of the as-synthesized MAPbI₃ and FAPbI₃, and the diffraction peaks are fairly consistent with the reported literatures. All characteristic diffraction peaks of MAPbI₃ are observed at angles of 28.1°, 28.4°, 31.9°, 40.4° and 43.0°, which are indexed to (004), (220), (310), (224), and (314) reflections, respectively. Normally, FAPbI₃ has two isomers including a black and a yellow perovskite phase with different crystal structure.³⁰ The former perovskite phase corresponds to trigonal symmetry (P3m1), and its characteristic peaks are at 14.0°, 28.0°, 31.4°, 40.0°, 42.5°, which are similar with that of tetragonal MAPbI₃. While the latter attributes to P63mc layered crystal structure.^{23,24} Obviously, only the black phase can absorb adequate light to bring high efficiencies. It appears that the black P3m1 phase is stable at higher temperatures of 70°C while it fully converts to yellow

phase in a humid atmosphere at room temperature quickly.

FAPbI₃ perovskite on TiO₂ film with one-step spin-coating method changed to the dark colour at temperatures over 140 °C but with poor reproducibility. This high annealing temperature of one-step spin-coating method may result in a poor crystal quality FAPbI₃ perovskite layer, which may lead to deterioration of the devices performance once assembled in solar cells.^{24, 27} Therefore, sequential deposition method was used to fabricate the devices so as to decrease the fabricating temperature. In order to verify the crystalline situation in the devices, the XRD patterns of blank TiO₂/ZrO₂/carbon film and PbI₂ in TiO₂/ZrO₂/carbon film, MAPbI₃ and FAPbI₃ based cells by sequential deposition method were characterized. As illustrated in Figure 2b, nearly all the PbI₂ in the devices converts to MAPbI₃ and FAPbI₃ respectively. The diffraction peaks agree well with samples on the glass substrate. For FAPbI₃ based cell, XRD reflections at 24.2°, 28.0°, 31.4°, 40.1°, and 42.7° are indexed to (202), (220), (222), (400), and (330) reflections, respectively, corresponding to the black polymorph of FAPbI₃.²⁷

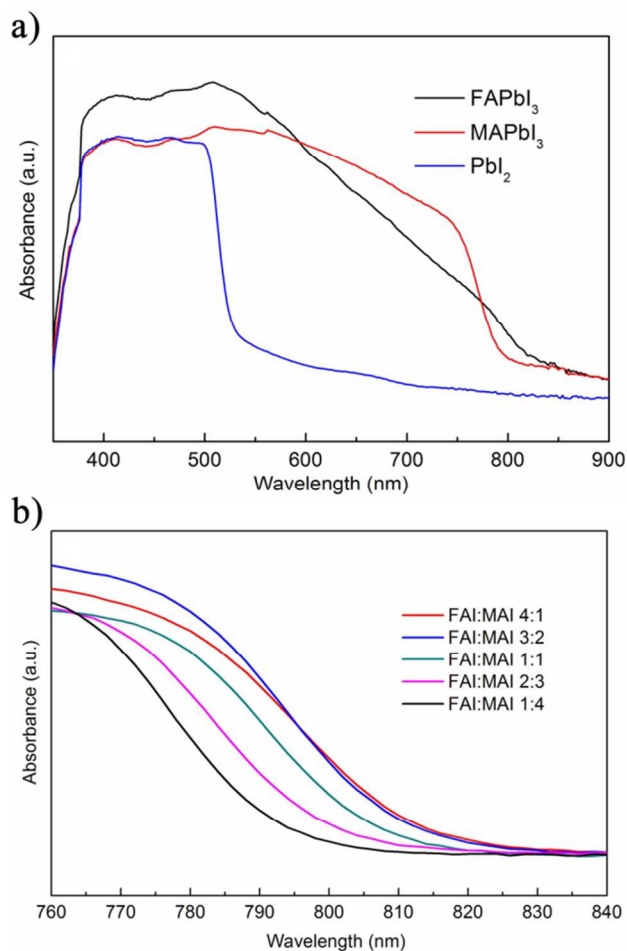


Figure 3 (a) The UV-visible absorption spectra of PbI₂, MAPbI₃ and FAPbI₃ on TiO₂ films from 350nm to 900nm by sequential deposition method; (b) The UV-visible absorption spectra of (FA)_x(MA)_{1-x}PbI₃ (x=0.2, 0.4, 0.5, 0.6, 0.8,) on TiO₂ films from 760nm to 840nm by sequential deposition method.

Figure 3a presents the absorption spectra of PbI₂, MAPbI₃ and

FAPbI₃ on TiO₂ films by sequential deposition method. The Pbl₂ sample shows absorption in the visible region ($\lambda < 500$ nm), presenting a bright yellow colour. After dipping in MAI or FAI solution respectively, the films turned to a dark colour for the forming of MAPbI₃ and FAPbI₃ perovskites. An obvious “cut-off” feature of FAPbI₃ after 840 nm indicates that bandgap absorption arises at around 840 nm, corresponding to energy of ca. 1.47 eV, which is in good agreement with previous observation.²⁵ While for MAPbI₃, the onset of the absorption

spectra is 800 nm, stemming from the larger band-gap of 1.55 eV.³¹ The lower bandgap of FAPbI₃ makes it absorb light over 800nm and convert to current a greater proportion of the sun’s spectrum compared with MAPbI₃. It is worth noting that the absorbance of FAPbI₃ reduces faster than that of MAPbI₃ in the range of 600 to 840 nm, suggesting a decreased light-harvesting ability in this range.²⁷

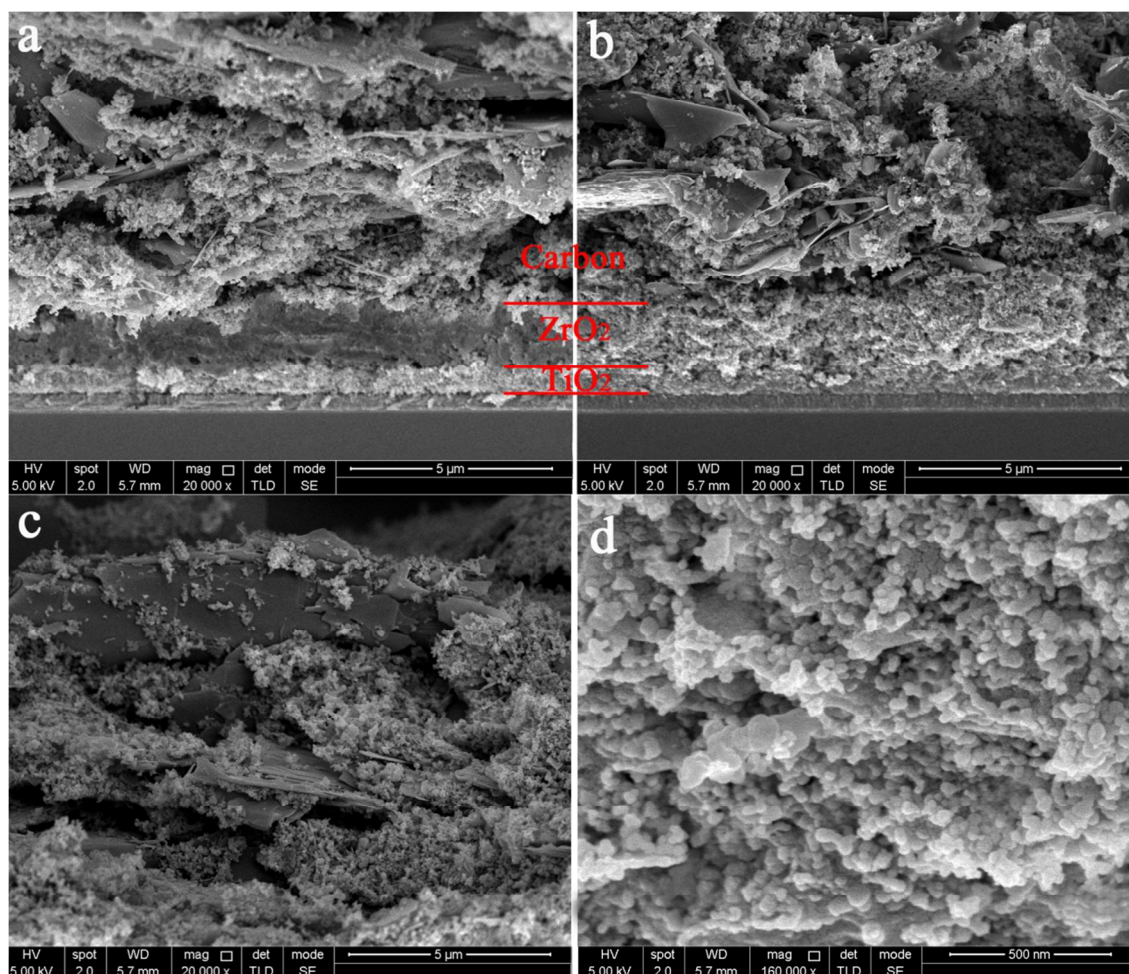


Figure 4 (a) Scanning electron microscopy (SEM) image from the cross section of the blank TiO₂/ZrO₂/carbon film; (b) The cross section of the mesoscopic solar cell with FAPbI₃; (c) The surface morphology of blank carbon layer; (d) The high magnification of FAPbI₃ coated TiO₂/ZrO₂ film.

Table 1 Photoelectric parameters of mesoscopic solar cells with MAPbI₃, FAPbI₃ and (FA)_{0.6}(MA)_{0.4}PbI₃ under 100 mW cm⁻² AM 1.5G illumination.

Perovskite	J_{SC} (mA cm ⁻²)	V_{OC} (mV)	FF	PCE (%)
MAPbI ₃	17.5±0.3	928±10	0.70±0.02	11.4±0.3
FAPbI ₃	18.4±0.2	901±12	0.72±0.02	11.9±0.2
(FA) _{0.6} (MA) _{0.4} PbI ₃	20.9±0.3	921±8	0.67±0.02	12.9±0.2

Figure 4a presents the scanning electron microscopy (SEM) images from the cross section of the blank TiO₂/ZrO₂/carbon films. The thicknesses of TiO₂ and ZrO₂ layers are approximately 700 nm and 1.5 μm, respectively. While for the thickness of carbon layer, it is 10 μm. Figure 4b and 4d show the cross section of the solar cell filled with FAPbI₃ perovskite and the high

magnification of FAPbI₃ coated TiO₂/ZrO₂ film, respectively. It is clear that FAPbI₃ perovskite is filled fully across the mesoporous TiO₂ and ZrO₂ layers, which makes it difficult to identify the boundary between TiO₂ and ZrO₂ layers. This will result of an efficient electron transfer from the perovskite to TiO₂ or across it.³² Figure 4c shows the morphology of carbon layer without infiltrating perovskite on top view, we can see that the large flaky graphite are well enclosed by the small carbon black particles and the thick porous carbon film adheres well with the ZrO₂ layer. The rough mesoporous surface of the carbon CE will be benefit for the infiltration of different size of cubic MAPbI₃ or FAPbI₃ perovskites.¹⁶

The $J-V$ curves of the mesoscopic perovskite solar cells are shown in Figure 5a and the corresponding photovoltaic parameters are summarized in Table 1. With a sequential

deposition method, the MAPbI₃ based device achieves PCE of 10.4% with J_{SC} of 17.5 mA cm⁻², V_{OC} of 928 mV, and fill factor (FF) of 0.70 at the light illumination of 100 mW cm⁻² AM 1.5G. Under the same condition, the FAPbI₃ device shows a higher PCE of 11.9% with J_{SC} of 18.4 mA cm⁻², V_{OC} of 901 mV and FF of 0.72. The increased efficiency should be mainly attributed to the increase of J_{SC} from 17.5 mA cm⁻² to 18.4 mA cm⁻², offsetting the decreased 27 mV V_{OC} of the FAPbI₃ based device. As presented IPCE spectra in Figure 5b, the FAPbI₃ perovskite solar cell successfully generates photocurrent up to 840nm, rather than only 800 nm achievable with the MAPbI₃ perovskite, due to the narrower bandgap. The shape of the IPCE spectra agrees well with its absorption spectra, and IPCE reaches the maximum in the range of 400-550 nm of over 65%. The integration of the IPCE spectra gives 16.3 mA cm⁻² for the MAPbI₃ and 17.3 mA cm⁻² for the FAPbI₃, which is rather in good agreement with the J_{SC} obtained from the J - V curves. Note that IPCE is lower for FAPbI₃ than for MAPbI₃ at long wavelength longer than 600 nm, which should be mainly ascribed to the relatively weak light absorption by FAPbI₃ at long wavelength region compared to MAPbI₃.

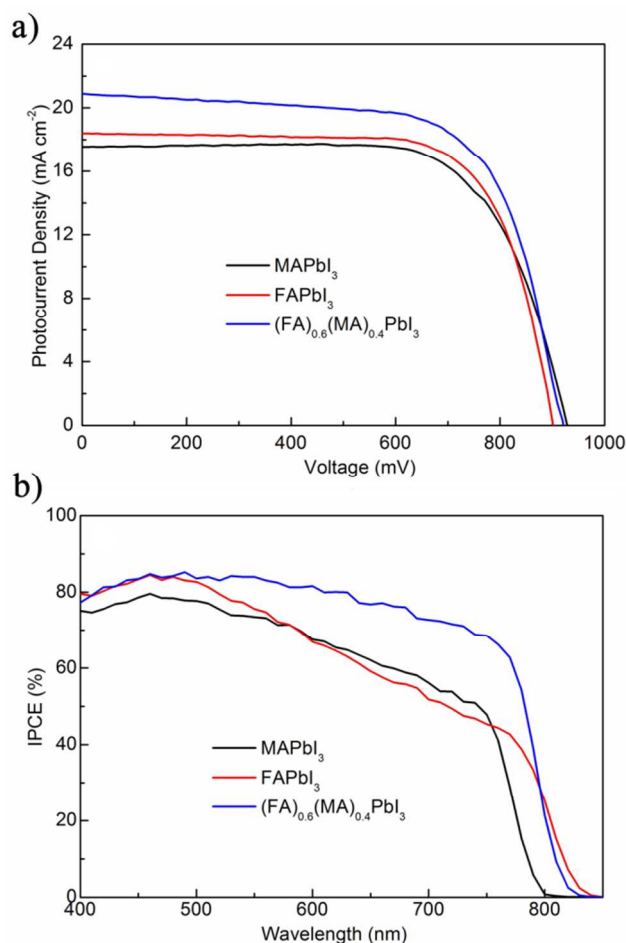


Figure 5 (a) J - V curves of mesoscopic perovskite solar cells with MAPbI₃, FAPbI₃ and (FA)_{0.6}(MA)_{0.4}PbI₃ under 100 mW cm⁻² AM 1.5G illumination; (b) The corresponding IPCE spectra.

To compensate the IPCE loss from 600-750 nm of FAPbI₃ and further improve the efficiency of solar cells, the FAI was mixed with MAI in solution to form (FA)_x(MA)_{1-x}PbI₃ perovskite.^{26, 27}

The absorption spectra of (FA)_x(MA)_{1-x}PbI₃ for various ratios in the range of 760 nm to 840 nm are presented in Figure 3b. It is obvious that the absorption onset of the perovskite is shifted gradually to longer wavelength as the content of FAI is increased. At the FAI/MAI ratio of 3:2 and 4:1, the films show broader light harvesting and higher absorbance with both merits of MAPbI₃ and FAPbI₃, inspiring us to improve the performance of the devices with mixed MAPbI₃ and FAPbI₃ perovskite. As shown in Figure 5 and Table 1, with a FAI/MAI ratio of 3:2 namely (FA)_{0.6}(MA)_{0.4}PbI₃, fully printable mesoscopic perovskite solar cell with carbon CE shows the highest J_{SC} of 20.9 mA cm⁻², with V_{OC} of 921 mV, FF of 0.67 and PCE of 12.9%. As far as we know, this is the highest efficiency of hole-conductor-free, fully printable perovskite solar cell with carbon CE. The increased PCE of the devices should be mainly attributed to the significantly increased J_{SC} relative to pure FAPbI₃ and MAPbI₃, while the high V_{OC} and FF were nearly maintained. A hysteresis effect often appears during measurement of the J - V curves of perovskite solar cells. For the mesoscopic solar cells with sequential deposition method, one device based on (FA)_{0.6}(MA)_{0.4}PbI₃ perovskite was measured with different scanning rates forward or backward carefully. The difference in efficiency is lower than 1% between forward and backward scanning with the scan rate no more than 250 mV s⁻¹ (Figure S1). The IPCE of the cell with (FA)_{0.6}(MA)_{0.4}PbI₃ in Figure 5b exceeds the values of the two pure perovskites from 400 to 800 nm and the onset is between FAPbI₃ and MAPbI₃ in accordance with the absorbance spectra. Integration of the IPCE yields J_{SC} of 20.1 mA cm⁻² for (FA)_{0.6}(MA)_{0.4}PbI₃.

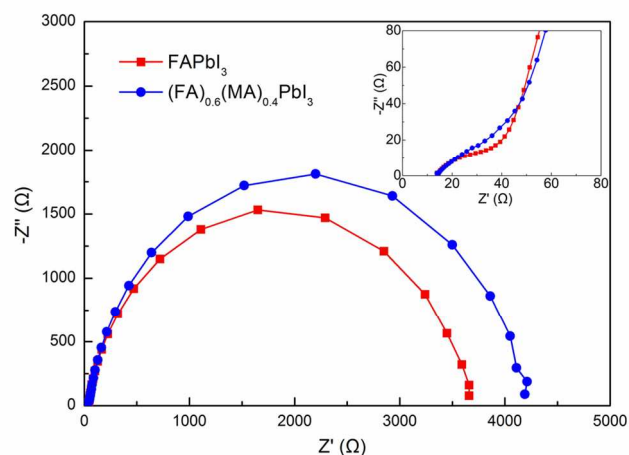


Figure 6 Nyquist plots of mesoscopic perovskite solar cells with FAPbI₃ and (FA)_{0.6}(MA)_{0.4}PbI₃ in the dark with a bias of 0.6 V. The inset is a zoom of the low impedance region.

To further investigate the charge transport process in the devices, electrochemistry impedance spectroscopy (EIS) were measured for FAPbI₃ and (FA)_{0.6}(MA)_{0.4}PbI₃ perovskite solar cells. Based on our previous report,¹⁵ there are two RC elements representing charge transfer resistance and recombination at Perovskite/CE and TiO₂/Perovskite interfaces in our EIS spectra. In the EIS measurements, when the forward applied bias was decreased, the first semicircle at high frequency region remained almost unchanged, while the second semicircle at low frequency

increased in diameter, as shown in Figure S2. Figure 6 shows the Nyquist plots of devices based on FAPbI₃ and (FA)_{0.6}(MA)_{0.4}PbI₃, and the inset is a zoom of the low impedance region. Similar semicircles in the high frequency suggest similar charge transfer resistances at Perovskite/CE interface. Besides, it can be seen that the radius of the semicircle in the low frequency is larger for (FA)_{0.6}(MA)_{0.4}PbI₃ based device compared with FAPbI₃ based device, which indicates less recombination at TiO₂/perovskite interface. This result corresponds to the differences of V_{OC} in Table 1. It was reported that when FAPbI₃ and MAPbI₃ were combined, the defects in the perovskite were reduced²⁷ thus leading to less recombination. On the other hand, the conduction band of (FA)_{0.6}(MA)_{0.4}PbI₃ is likely to increase due to higher bandgap compared with pure FAPbI₃ (indicated by UV-visible absorption spectra), which in turn can lead to a reduced recombination and an increased V_{OC} . More physical mechanism should be further study.

Conclusions

In summary, high efficient hole-conductor-free mesoscopic perovskite solar cells with carbon CE based on formamidinium lead iodide HC(NH₂)₂PbI₃ were successfully fabricated. It is demonstrated that FAPbI₃ successfully formed a cubic perovskite structure across the three mesoporous layers of TiO₂/ZrO₂/carbon films characterized by XRD spectra. The pure FAPbI₃ based solar cell showed extended IPCE up to 840nm. With sequential deposition method, a high PCE of 11.9% was obtained for FAPbI₃ based solar cell. By optimizing the FAI/MAI mole ratio to 3:2, the J_{SC} was enhanced to 20.9 mA cm⁻², which brought a superior PCE of 12.9%. As far as we know, this is the highest efficiency of hole-conductor-free fully printable perovskite solar cells. Nevertheless, there still remains room for further substantial improvement in the photovoltaic parameters by doping or optimizing the structure of the devices. Finally, these results show that the fully printable fabrication process and low cost of the devices are extremely promising in the future development and industrialization of photovoltaic cells.

Acknowledgement

The authors acknowledge the financial support from the Ministry of Science and Technology of China (863 program, No. SS2013AA50303), the National Natural Science Foundation of China (Grant No. 61474049, 61106056), the Science and Technology Department of Hubei Province (No. 2013BAA090), and the Fundamental Research Funds for the Central Universities (HUSTNY022). We also thank the Analytical and Testing Center of Huazhong University of Science and Technology (HUST) for X-ray diffraction (XRD) and field emission scanning electron microscopy (FESEM) testing.

Notes and references

Michael Grätzel Center for Mesoscopic Solar cells, Wuhan National Laboratory for Optoelectronics, School of Optical and Electronic Information, Huazhong University of Science and Technology, Wuhan, Hubei, P.R. China, 430074. E-mail: hongwei.han@mail.hust.edu.cn; Tel:

+86 27 8779 3027

- Electronic Supplementary Information (ESI) available: [$J-V$ curves of perovskite solar cell; Impedance spectroscopy measurements].
- H. J. Snaith, *J. Phys. Chem. Lett.*, 2013, **4**, 3623–3630.
 - M. Liu, M. B. Johnston and H. J. Snaith, *Nature*, 2013, **501**, 395–398.
 - J. Burschka, N. Pellet, S.-J. Moon, R. Humphry-Baker, P. Gao, M. K. Nazeeruddin and M. Grätzel, *Nature*, 2013, **499**, 316–319.
 - S. Kazim, M. K. Nazeeruddin, M. Grätzel, S. Ahmad, *Angew. Chem., Int. Ed.*, 2014, **53**, 2812–2824;
 - P. K. Nayak, D. Cahen, *Adv. Mater.*, 2014, **26**, 1622–1628.
 - P. Gao, M. Grätzel and M. K. Nazeeruddin, *Energy Environ. Sci.*, 2014, **7**, 2448–2463
 - M. A. Green, A. and H. J. Snaith, *Nat. Photonics*, 2014, **8**, 506–514.
 - M. D. McGehee, *Nat. Photonics*, 2013, **501**, 323–325.
 - N. G. Park, *J. Phys. Chem. Lett.*, 2013, **4**, 2423–2429.
 - M. Loi and J. Hummelen, *Nat Mater*, 2013, **12**, 1087–1089
 - S. Aharon, B. Cohen, and L. Etgar, *J. Phys. Chem. C*, 2014, **118**, 17160–17165.
 - S. Aharon, S. Gamliel, B. Cohen and L. Etgar, *Phys. Chem. Chem. Phys.*, 2014, **16**, 10512.
 - J. Shi, J. Dong, S. Lv, Y. Xu, L. Zhu, J. Xiao, X. Xu, H. Wu, D. Li, Y. Luo and Q. Meng, *Appl. Phys. Lett.*, 2014, **104**, 063901.
 - Z. Ku, Y. Rong, M. Xu, T. Liu and H. Han, *Sci. Rep.*, 2013, **3**, 3132.
 - Y. Rong, Z. Ku, A. Mei, T. Liu, M. Xu, S. Ko, X. Li, and H. Han, *J. Phys. Chem. Lett.*, 2014, **5**, 2160–2164.
 - H. Wang, G. Liu, X. Li, P. Xiang, Z. Ku, Y. Rong, M. Xu, L. Liu, M. Hu, Y. Yang and H. Han, *Energy Environ. Sci.*, 2011, **4**, 2025–2029.
 - M. Hu, J. Sun, Y. Rong, Y. Yang, L. Liu, X. Li, M. Forsyth, D. Macfarlane and H. Han, *J. Power Sources*, 2014, **248**, 283–288.
 - Z. Li, S. Kulkarni, P. Boix, E. Shi, A. Cao, K. Fu, S. Batabyal, J. Zhang, Q. Xiong, L. Wong and et al., *ACS Nano*, 2014, **8**, 6797–6804.
 - H. J. Snaith, *Adv. Funct. Mater.*, 2010, **20**, 13–19.
 - Y. Ogomi, A. Morita, S. Tsukamoto, T. Saitho, N. Fujikawa, Q. Shen, T. Toyoda, K. Yoshino, S.S. Pandey, and T. Ma, *J. Phys. Chem. Lett.*, 2014, **5**, 1004–1011.
 - F. Hao, C.C. Stoumpos, R.P. Chang and M.G. Kanatzidis, *J. Am. Chem. Soc.*, 2014, **136**, 8094–8099.
 - F. Hao, C. Stoumpos, D.Cao, R. Chang and M. Kanatzidis, *Nat. Photonics*, 2014, **8**, 489–494.
 - T. Koh, K. Fu, Y. Fang, S. Chen, T. Sum, N. Mathews, S. Mhaisalkar, P. Boix and T. Baikie, *J. Phys. Chem. C*, 2014, **118**, 16458–16462.
 - S. Pang, H. Hu, J. Zhang, S. Lv, Y. Yu, F. Wei, T. Qin, H. Xu, Z. Liu and G. Cui, *Chem. Mater.*, 2014, **26**, 1485–1491.
 - G. Eperon, S. Stranks, C. Menelaou, M. Johnston, L. Herz and H. Snaith, *Energy Environ. Sci.*, 2014, **7**, 982–988.
 - N. Pellet, P. Gao, G. Gregori, T. Y. Yang, M. K. Nazeeruddin, J. Maier and M. Grätzel, *Angew. Chem., Int. Ed.*, 2014, **53**, 3151–3157.
 - J. Lee, D. Seol, A. Cho, and N. Park, *Adv. Mater.*, 2014, **26**, 4991–4998.
 - A. Kojima, K. Teshima, Y. Shirai and T. Miyasaka, *J. Am. Chem. Soc.*, 2009, **131**, 6050–6051.

29. M. Xu, Y. Rong, Z. Ku, A. Mei, T. Liu, L. Zhang, X. Li and H. Han, *J. Mater. Chem. A*, 2014, **2**, 8607-8611.
30. C. C. Stoumpos, C. D. Malliakas and M. G. Kanatzidis, *Inorg. Chem.*, 2013, **52**, 9019-9038.
- 5 31. H. Kim, C. Lee, J. Im, K. Lee, T. Moehl, A. Marchioro, S. Moon, R. Humphry-Baker, J. Yum, J. Moser, M. Grätzel and N. Park, *Sci. Rep.*, 2012, **2**, 591.
32. T. Leijtens, B. Lauber, G. E. Eperon, S. D. Stranks and H. J. Snaith, *J. Phys. Chem. Lett.*, 2014, **5**, 1096-1102.
- 10 33. G. D. Niu, W. Z. Li, F. Q. Meng, L. D. Wang, H. P. Dong and Y. Qiu, *J. Mater. Chem. A*, 2014, **2**, 705-710.
34. T. Leijtens, G. E. Eperon, S. Pathak, A. Abate, M. M. Lee and H. J. Snaith, *Nat. Commun.*, 2013, **4**, 2885.